Liquid Crystals
Publication details, including instructions for authors and subscription information:
http://www.informaworld.com/smpp/title~content=t713926090

Relaxation dispersion and zero-field spectroscopy of thermotropic and lyotropic liquid crystals by fast field-cycling N.M.R.

F. Noack[a]; M. Notter[a]; W. Weiss[a]
[a] Physikalisches Institut der Universitat Stuttgart, Stuttgart 80, F.R. Germany

To cite this Article Noack, F. , Notter, M. and Weiss, W.(1988) 'Relaxation dispersion and zero-field spectroscopy of thermotropic and lyotropic liquid crystals by fast field-cycling N.M.R.', Liquid Crystals, 3: 6, 907 — 925
To link to this Article: DOI: 10.1080/02678298808086548
URL: http://dx.doi.org/10.1080/02678298808086548

LIQUID CRYSTALS, 1988, VOL. 3, NOS. 6 AND 7, 907–925

Invited Article

Relaxation dispersion and zero-field spectroscopy of thermotropic and lyotropic liquid crystals by fast field-cycling N.M.R.

by F. NOACK, M. NOTTER and W. WEISS
Physikalisches Institut der Universität Stuttgart, Pfaffenwaldring 57, 7000 Stuttgart 80, F.R. Germany

Systematic field-cycling measurements of the T_1 relaxation dispersion in numerous nematic liquid crystals (azoxybenzenes, Schiff's bases, biphenyls, phenyl-cyclohexanes, cyclo-cyclo-hexanes) confirm our previous observations obtained for PAA and MBBA that order fluctuations of the nematic director are a significant relaxation contribution only at low Lamor frequencies ν, i.e. far below the usual megahertz range. Their significance is demonstrated most convincingly by the characteristic square-root dispersion law, $T_1 \sim \nu^{1/2}$, which occurs in the kilohertz range and which completely disappears above the nematic–isotropic phase transition. The strength of the collective relaxation mechanism varies by more than two orders of magnitude in the sequence (selection) PAA-d_8, PAA, PAA-d_6, PAB, OCB7, MBBA, CB7, PCH7, MBBA-d_6, MBBA-d_{13} and CCH7. This finding can be understood almost quantitatively by the widely differing separations and orientations of proton pairs on the molecules, together with the different viscoelastic parameters of the nematogens. In addition, the underlying slow molecular reorientations have been observed in MBBA and PAA by intensity changes of the zero-field spectra, which are absent for high-field measurements. Similarly, smectic type order fluctuations in layered liquid crystal structures prove to be an effective relaxation mechanism only at low Lamor frequencies. This has been verified by the related linear relaxation dispersion profile, $T_1 \sim \nu^1$, for both thermotropic systems (TBBA, C_{12}-AA) and lamellar lyotropic mixtures (e.g. potassium laurate in water and phospholipids in water). Our results concerning the time scale of the $T_1 \sim \nu^{1/2}$ and $T_1 \sim \nu^1$ regime do not agree with conclusions drawn from conventional high-field techniques.

1. Introduction: Why field-cycling measurements of order and order fluctuations in liquid crystals?

Measurements of the molecular order in liquid crystals by the line splittings of proton, deuteron or carbon N.M.R. spectra are now a standard procedure. The basic idea of this analysis is well-known since the early sixties from the pioneering work of Lippmann *et al.* [1] and of Saupe *et al.* [2]. However looking closer at the details of the ordering still reveals many unsolved questions, in particular with respect to the time scale or fluctuation of the order; in other words details of the related collective molecular reorientations are rather unclear.

In 1969 Pincus [3] and Blinc *et al.* [4] predicted independently that a special kind of order fluctuation, now called order fluctuation of the nematic director (OFD or OFN), should lead to a characteristic square-root dependence of the longitudinal proton relaxation time T_1 on the Larmor frequency ν ($\equiv \omega/2\pi$). The various modes of the fluctuation with a distribution of wave-vectors involve a broad spectrum of

reorientational time constants and thus entail a rather unusual $T_1(\nu)$ profile. This famous $T_1 \sim \nu^{1/2}$ law for the relaxation dispersion in nematic liquid crystals, and later refinements by more sophisticated calculations [5], have initiated countless experimental studies to verify such collective motions in almost any type of available liquid-crystalline mesophase. Such studies have met only with limited success so far, and with rather conflicting conclusions, essentially for three reasons:

(i) As expected from standard relaxation theory [6], in liquid crystals there may exist numerous non-collective segmental or overall molecular reorientations which make it difficult to separate unambiguously the $\nu^{1/2}$-law from other contributions.

(ii) As known from several extensions of the Pincus–Blinc model, in particular by systematic calculations of Vilfan and Žumer [7, 8], there may exist a variety of collective motions, which cause quite different forms of the T_1 frequency dependence. For instance, if we take the dimensionality of the dynamics into account, we find $T_1 \sim \nu^{1/2}$, $T_1 \sim \nu^{2/2}$ or even $T_1 \sim \nu^{3/2}$ for OFD modes propagating in three, two or one dimensions, respectively. So we have to disentangle more than a single exponent eventually related to order fluctuations!

(iii) Last but not least, the main part of the collective motions should be slow compared to the Lamor frequency range of standard N.M.R. spectrometers because of the large number of particles concerned. This makes them a rather ineffective relaxation contribution in the conventional megahertz regime, and consequently common apparatus seems not very adequate to observe such processes.

The first and second problem are intrinsic and cannot be avoided in general, but the last one can be overcome by extending the relaxation dispersion measurements to much lower, even to zero Larmor frequency, namely through further decreasing the external Zeeman field. Now the critical point of direct low-field experiments is the inherently poor sensitivity caused by Curie's law, and so it is necessary to enhance the signal by suitable means. The most transparent and elegant way is to prepare a high magnetization by cycling the Zeeman field between high and low levels, in short, field-cycling [9, 10]; unfortunately this involves some technical problems. Up to the moment they have prevented the method to become very familiar. In a simple form field-cycling was first applied by Pound in 1951 [11], but the basic practical concepts were suggested much later by Redfield *et al.* in 1968 [12].

Based on the pioneering work of Redfield several research groups [9, 10] have tried in the past 20 years to make field-cycling techniques more powerful and versatile. In this contribution we describe briefly the present capabilities, together with selected applications to liquid crystals, where the method proves particularly unwieldy because of the $\nu^{1/2}$ or often even a stronger T_1 divergence. First, it will be illustrated how it has become possible to switch high Zeeman fields (the magnetic flux density B) of more than 1 T in less than half of a millisecond with adequate accuracy. Then we review field-cycling measurements of both the relaxation dispersion and of zero-field spectra for some nematic, smectic and lyotropic liquid crystals. These materials generally require such fast cycling techniques in order to observe low-field signals

of protons or deuterons, and then eventually to detect a square-root or another relaxation dispersion profile attributable to order fluctuations.

2. A powerful field-cycling device

Let us recall briefly the principle of field-cycling experiments [9, 10] (see figure 1) and describe some recent instrumental developments [13, 14]. In order to observe N.M.R. with satisfactory sensitivity in a low, variable Zeeman field B_0, here denoted the evolution field B_{0E}, the Zeeman field is not maintained constant as usual but modulated in a special way. The spins are polarized and detected with B_0 as high as possible (B_{0P}, B_{0D}), and the desired evolution field is inserted only for a small interval. If the transit times from high to low (t_{off}) and from low to high (t_{on}) are made sufficiently fast, so that no magnetization is lost or changed, any N.M.R. experiment can be performed field dependent with almost the same sensitivity as a conventional high-field measurement. For liquid crystals, the longitudinal relaxation time is often of the order of 1 to 10 ms, and therefore both transits must not exceed this time significantly, that means they must be rather short.

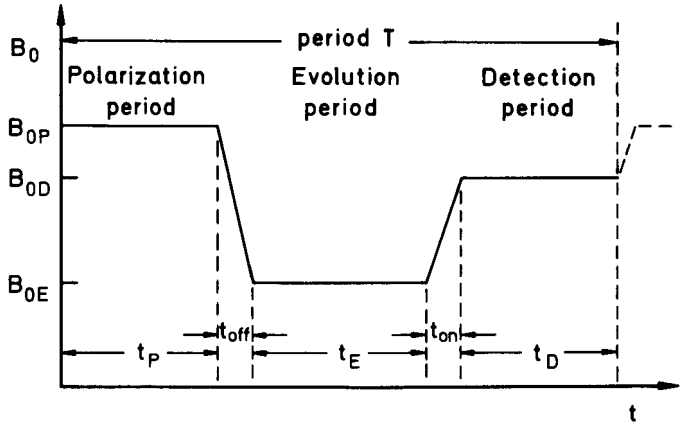

Figure 1. Typical modulation of the Zeeman field B_0 in a field-cycling N.M.R. experiment. The critical parameters are the values of the maximum polarization and detection fields (B_{0P}, B_{0D}) and the shortest possible transit times (t_{off}, t_{on}) to and from the evolution field level (B_{0E}).

Originally [11], the field-cycle was produced mechanically by moving or shooting the sample between a strong and a weak magnet. This method is relatively simple, but it has many drawbacks; above all it is generally too slow (typical: $t_{on} \approx t_{off} \geqslant 0{\cdot}1$ s) for work with liquid crystals. The more powerful alternative [12] (see figure 2) is to produce the transits by quickly turning on or off the current of a power supply through a magnet coil, i.e. to use an electronic switch. To understand the main technical difficulties we have to consider some details. If a voltage U is applied to a coil with inductance L and series resistance R_s, the current I increases exponentially with time constant L/R_s. This exponential increase (see figure 3) leads to an equilibrium state more rapidly the higher the damping resistance, and thus often to the incorrect statement that the switch becomes fast with increasing value of R_s. Almost the opposite is the case; the fastest current increase $(dI/dt)_{max} = U/L$ is independent on the value of R_s, and the maximum slope U/L is maintained longer, the smaller the

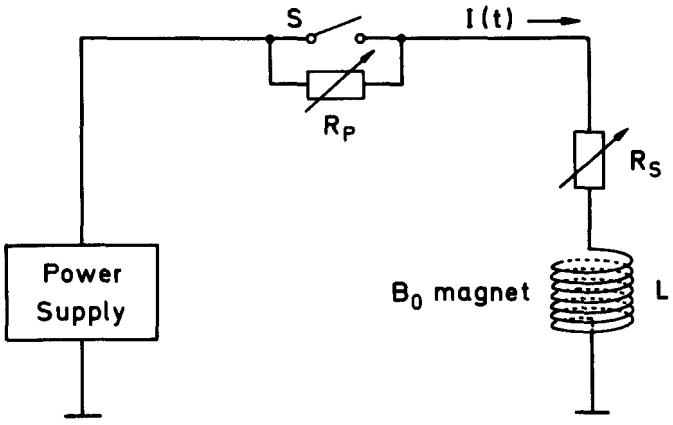

Figure 2. Basic components of an electronic field-cycling switch: Power supply, transistor switch and magnet coil (inductance L, series resistance R_s).

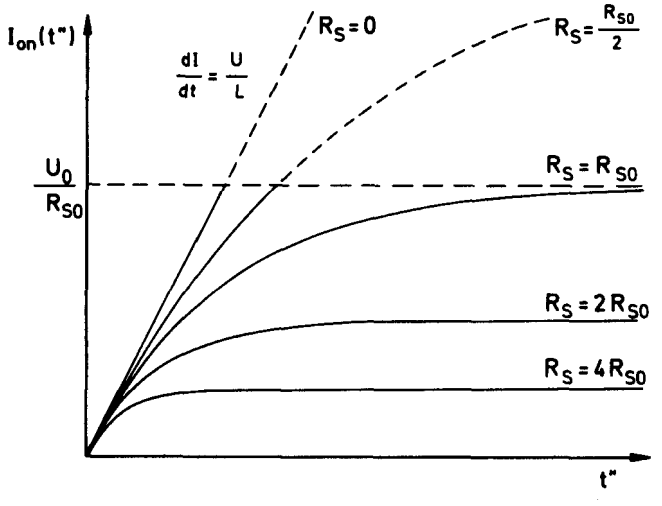

Figure 3. Current characteristic $I(t)$ of a magnet coil with inductance L and variable series resistance R_s after applying a constant driving voltage U.

value of R_s. In principle, a cryomagnet with $R_s = 0$ gives a better $I(t)$ characteristic than a normal conducting coil.

So to obtain a fast field-cycling switch we must be concerned with high *voltages U* and magnets with *small inductance L* and *resistance* R_s. This was already known by Redfield, but he did not have the electronic or mechanical components to build a powerful and versatile cycling network. These means are now available. On the one hand by modern semiconducting devices such as MOSFET's (metal-oxide-semiconductor-fieldeffect-transistors) and GTO's (gate-turn-off thyristors), which allow us to control conveniently high electric currents at voltages of more than 1 kV [13]; on the other hand by the possibility to build small low-inductance and low-ohmic coils by computer controlled cutting from copper cylinders [14]. Making use of such modern technical developments, we have recently improved our field-cycling spectrometers considerably, towards higher detection fields (presently 1·2 T) and towards

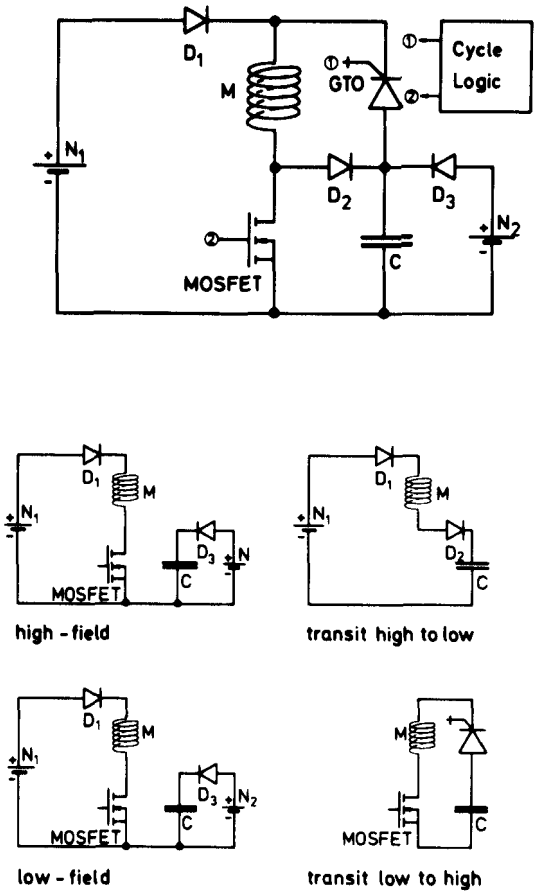

Figure 4. Concept of a high-power MOSFET–GTO switch network for fast field-cycling experiments.

faster transits (presently 0·4 ms), by what we call the MOSFET–GTO switch (see figure 4). It allows us to measure the relaxation dispersion of liquid crystals for protons, and, in the near future, also for deuterons, with T_1 less than about 1 ms. The switch operates approximately as follows [10, 13]: the current through the magnet coil of a 400 A/125 V/50 kW supply N_1 is controlled by a MOSFET network, which tolerates voltage peaks up to 1·2 kV without being damaged. To reduce the current, the MOSFET gate voltage is regulated to a desired level and the decreasing current is driven on a capacitance C, the energy storage capacitance, which is precharged by a high voltage supply N_2. This supply provides a voltage adjustable up to 1·2 kV so that the ratio U/L can be made much larger than by the current source N_1, and consequently the speed of the current reduction becomes very fast. Similarly, to turn on the current through the magnet, the MOSFET gates are opened again, and simultaneously the high-voltage of the storage capacitance is connected to the coil with the correct polarity by firing a 400 A/1·5 kV GTO thyristor. Therefore, the increase is driven by the same large voltage U as the decrease. As soon as the level of the detection field is reached, the GTO is turned off and the MOSFETs stabilize the current at a steady state. Obviously, the device transforms the magnetic coil energy to an electric field energy and vice versa, so that the average power to

produce the field-cycle is rather small. Only the losses in the magnet have to be compensated.

The most critical components of the field-cycling circuit are the storage capacitance and the magnet coil. So let us conclude this instrumental overview with some remarks on these novel parts. To avoid significant voltage drops during the transits, the network makes use of a 10 000 μF/1·2 kV capacitance, which in both switching intervals provides a peak electric power of 400 A × 1200 V = 0·48 MW [13]. Since the cycle is repeated only once every second, the average power is at least about three orders of magnitude smaller. The coil is a very small, homogenized Kelvin-type magnet (length: 10 cm; bore: 2·6 cm; diameter: 7 cm), for which the variable conductor cross-sections were calculated by a Lagrange minimization formalism and then cut by a computer controlled lathe [14]. Such a construction, with variable cross-sections, allows us to produce from a given electric power the maximum field under accessory constraints on the homogeneity $\Delta B_0/B_0$ and the self-inductance L (presently: $B_{max} = 1{\cdot}2\,T$, $\Delta B_0/B_0 \leqslant 10^{-5}$, $L = 0{\cdot}4\,mH$). Together with appropriate freon cooling circuits the coil is oriented by a movable bearing along the direction of the earth's magnetic field to enable convenient field compensation and adjustments of low Larmor frequencies without any additional current loop.

A typical T_1 dispersion measurement proceeds quite conventionally (see figure 5). When the Zeeman field B_0 is cycled to a desired low level, the initial longitudinal

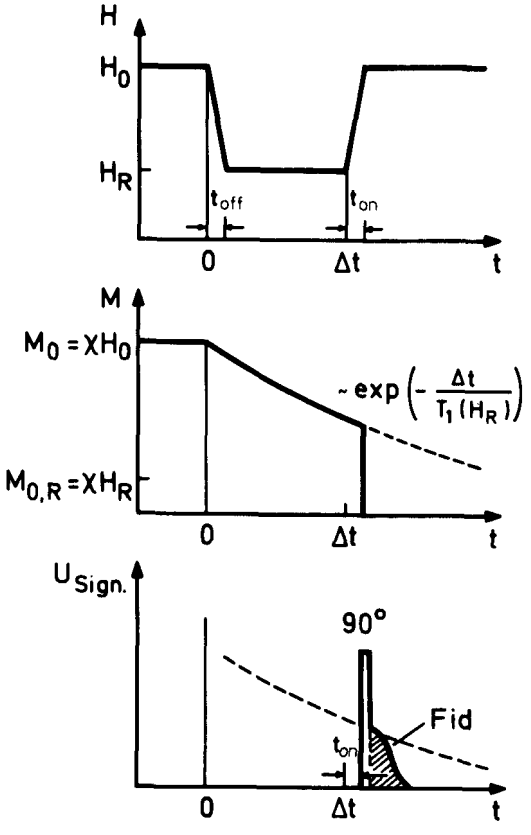

Figure 5. Principle of field or frequency dependent measurements of the longitudinal nuclear relaxation time T_1 by field-cycling techniques.

Table 1. Maximum flux densities (B_{max}) and minimum transit times (t_{off}, t_{on}) of some electronic field-cycling devices described in the literature.

B_{max} T	t_{off}, t_{on} ms	Reference
0·75	25	REDFIELD, A. G., FITE, W., and BLEICH, H. E., 1968, *Rev. scient. Instrum.*, **39**, 710. BROWN, R. D., and KOENIG, S. H., 1972, *IBM Res. Rep.*, RC 6712, Yorktown Heights.
0·47	20	ANDREANI, R., 1975, Thèse, Université de Grenoble.
0·25	3·5	STOHRER, M., and NOACK, F., 1977, *J. chem. Phys.*, **67**, 3729.
0·25	0·5	GRAF, V., 1980, Thesis, Universität Stuttgart.
0·88	'few'	KUMAGAI, K., and FRADIN, F. Y., 1983, *Phys. Rev.* B, **27**, 2770.
0·46	1·5	BLANZ, M., CHEN, G. Q., BIRLI, H., and MESSER, R., 1984, *Proc. 22nd Congress Ampere*, Zürich, p. 596.
1·5	30	VANDEMAELE, G., COPPENS, P., and VAN GERVEN, L., 1984, *Proc. 22nd Congress Ampere*, Zürich, p. 398.
0·40	2·0	GLOVER, K. J., 1986, Thesis, University of California.
1·25	20–30	SCHAUER, G., NUSSER, W., BLANZ, M., and KIMMICH, R., 1987, *J. Phys.* E **20**, 43.
1·20	0·4	SCHWEIKERT, K. H., KRIEG, R., and NOACK, F., *J. magn. Reson.* (submitted).
2·50	2·0	SCHWEIKERT, K. H., 1988, Thesis, Universität Stuttgart.

nuclear magnetization $M_0 = \chi H_0 = (\chi/\mu)B_0$ (χ: nuclear magnetic susceptibility, μ: magnetic permeability, H_0: magnetic field strength) decays exponentially with a time constant $T_1(H_R)$ characteristic of the Larmor frequency ν in the variable relaxation field $H_R = B_{0E}/\mu$. This decay is sampled as a function of time by a $\pi/2$ r.f.-pulse applied immediately after the transit to the high detection field. Then the procedure is repeated over the desired field range. All these steps are easily made computer controlled. Field dependent measurements of the transverse relaxation and the related spectra require a slightly more sophisticated B_0-cycle and more complex r.f.-pulse sequences [10, 15].

To honour the manifold contributions of other research groups to the improvement of electronic field-cycling techniques, and to compare our new capabilities with previous ones, table 1 presents some data on B_{0max} and $t_{on} \approx t_{off}$ from the literature. It shows how the switching times have been reduced in recent years, so that it is now possible, for the first time, to produce fields of more than 1 T with transit times below a millisecond. Through these improvements field-cycling relaxation dispersion measurements are no longer restricted to protons in liquid crystals but can now also be performed with deuterons, which was not possible previously either because of insufficient detection fields or because of too long transit intervals.

3. T_1 relaxation dispersion in thermotropic and lyotropic liquid crystals

What do we learn from such measurements? To illuminate the problem once again, let us first consider the basic theory and some old results obtained for the textbook nematogen PAA (para-azoxyanisole or 4,4′-dimethyloxyazoxybenzene). According to the simple Pincus–Blinc model, the effectiveness of the OFD relaxation contribution for a dipolar coupled spin pair on a nematic molecule depends on both molecular and macroscopic properties of the liquid crystal. On the one hand, on the magnetogyric ratio (γ) of the spins, the spin separation (d) in a pair, the spin pair

orientation (α) relative to the long molecular axis, the order parameter (S) of the long molecular axis, and the inclination (β) of the nematic director $\mathbf{n}$ with respect to the external field $\mathbf{B}_0$, parameters which describe the strength of the dipolar interaction. On the other hand, on the average Frank elastic constant (K), the average Miesowicz viscosity (η) and the absolute temperature (T) which measure the amplitudes and time constants of the director fluctuations. Explicitly the theory predicts a relaxation rate [3, 4, 5]

$$\frac{1}{T_{1\,\mathrm{OFD}}} = \frac{A_{\mathrm{OFD}}}{\nu^{1/2}} \tag{1a}$$

with

$$A_{\mathrm{OFD}} = \frac{9}{8\pi^{3/2}} \gamma^4 \hbar^2 k \frac{TS^2\eta^{1/2}}{d^6 K^{3/2}} \frac{(3\cos^2\alpha - 1)}{4} f(\beta), \tag{1b}$$

where $2\pi\hbar$ is the Planck constant, k is the Boltzmann constant, and usually $f(\beta) = f(0) = 1$. Evidently, in order to examine the concept of order director fluctuations we must be sure to be in the proper $\nu^{1/2}$ regime! That is the critical point in most N.M.R. work on this subject.

Immediately following the calculations by Pincus and by the group of Blinc [3, 4] that a dipolar coupled spin pair on a nematic liquid crystal, say on the benzene rings or on the methyl groups of PAA, should show a square-root law relaxation dispersion profile, several groups began to look for this unusual behaviour to study and analyse the various underlying parameters. Almost all early measurements believed to have found the crucial $\nu^{1/2}$ regime at megahertz Lamor frequencies using standard N.M.R. spectrometers [16]. But it can easily be shown that a square-root law fit over a narrow frequency range of 1 or 2 decades is almost meaningless due to the presence of other relaxation processes. In fact, when we extended such measurements (see figure 6) over a much broader interval by field-cycling techniques, we noticed first in the case of PAA that the true $\nu^{1/2}$-dispersion occurs at much lower values of ν, namely in the kHz and not in the MHz range [17, 18]. Note

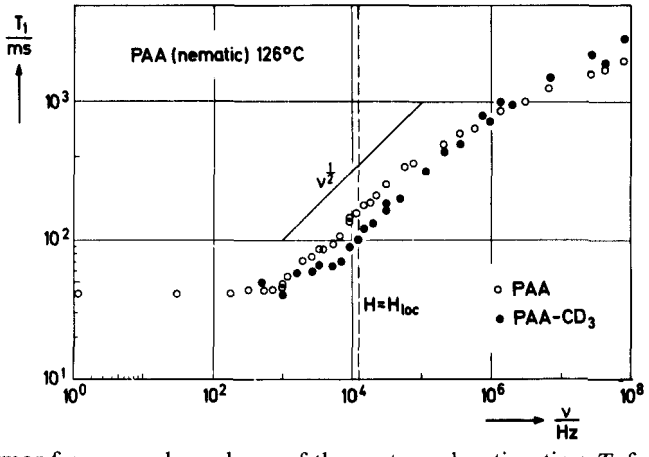

Figure 6. Larmor frequency dependence of the proton relaxation time T_1 for nematic PAA and PAA-d_6 [17, 18]. The square-root law is observed in the frequency range $10^3\,\mathrm{Hz} \lesssim \nu \lesssim 10^6\,\mathrm{Hz}$.

that even with a variation by a factor of 10^7 the disentanglement of competing contributions to T_1 is not easy for several reasons. On the one hand the high-field dispersion is often not very different from the $\nu^{1/2}$-law, and on the other hand a low-frequency plateau always develops, which complicates the $\nu^{1/2}$-dispersion profile. So a quantitative evaluation of the data has to consider numerous details not included in the simple Pincus–Blinc formula, as well as additional non-collective relaxation mechanisms.

When discussing qualitatively the significance of order fluctuations as possible relaxation contributions, it is particularly helpful to compare the nematic and isotropic phase [17, 18] (see figure 7). This view reveals, again for PAA as an example, that the low-field $\nu^{1/2}$-dispersion completely disappears above the nematic–isotropic transition temperature, whereas the high-field changes are comparatively small. The observed T_1 jump occurs within 0·1°C and hence nicely demonstrates where order and collective motions and where non-collective motions dominate the relaxation rate; the absence of orientational order lengthens T_1, only at frequencies $\nu \leqslant 10^6$ Hz.

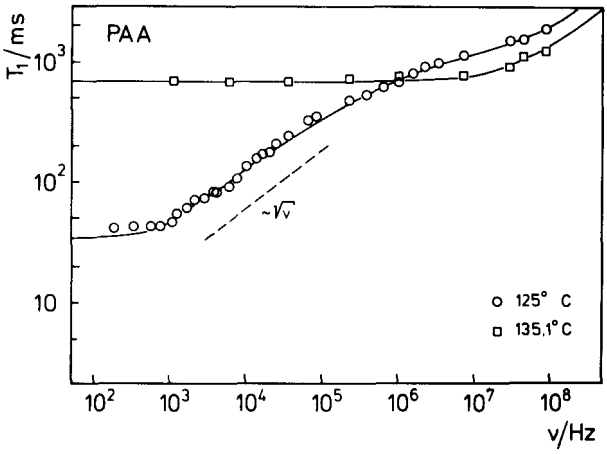

Figure 7. Comparison of the proton relaxation dispersion $T_1(\nu)$ for nematic and isotropic PAA [17, 18] showing the absence of the square-root law in the isotropic phase. The solid lines are model fits which, in addition to the OFD contribution including frequency cut-offs, take into account relaxation by self-diffusion, molecular rotation and by fluctuations of the order parameter S. Details are summarized in table 2.

A quantitative analysis of the $T_1(\nu)$ measurements for PAA and numerous other nematics like, for example, CB7 (4-*n*-heptyl-4′-cyanobiphenyl) (figure 8), PCH7 (4-(trans-4′-*n*-heptylcyclohexyl) benzonitrile)) (figure 9) and CCH7 (trans-4-(trans-4′-*n*-heptylcyclohexyl) cyclohexyl carbonitrile) (figure 10), which takes into account refinements of the Pincus–Blinc model (high- and low-frequency cut-offs [7, 19]) and further relaxation contributions (self-diffusion, molecular reorientations [10, 19]) supports the qualitative findings by reasonable magnitudes of the model parameters and systematic parallels. It shows three important aspects, namely:

(i) A curve fit to the proton measurements always reveals at least three relaxation mechanisms, with $T_{1\mathrm{OFD}}$ becoming significant for $\nu \leqslant 10^5 \ldots 10^6$ Hz. Some typical model parameters determined by such curve fits are listed in table 2.

Table 2. Relaxation formulae and model parameters used in the calculations of the curve fits of figures 7, 8, 9, 10, 11, 12 and 14. Note that the spectral densities $f_S(\nu, \tau_S)$ (self-diffusion) and $f_R(\nu, \tau_R)$ (rotation) [6, 10, 25] are normalized to give $f_S(\nu \to 0) = f_R(\nu \to 0) = 1$, whereas the frequency cut-off function $f_0(\nu/\nu_{cl})$ (order fluctuation) [5, 7, 19] is normalized by $f_0(\nu_{cl} \to 0) = 1$. Every curve is characterized by six model constants, namely by three relaxation amplitudes (A or B or C together with D and E), by the correlation times of self-diffusion and molecular rotation (τ_S, τ_R), and by the low cut-off frequency of the order fluctuation modes ($\nu_{cl} \equiv 1/(2\pi\tau_{OF})$). Due to the limited Larmor frequency range, the determination of the SD and R contributions is less accurate than that of the OF process.

$$\frac{1}{T_1(\nu)} = \frac{1}{T_{1OF}} + \frac{1}{T_{1SD}} + \frac{1}{T_{1R}}$$

Order fluctuation (OF)		
Nematic phase	$1/T_{1OF} = 1/T_{1OFD} = A\nu^{-1/2} f_0(\nu/\nu_{cl})$	[5, 7, 19]
Smectic phase	$1/T_{1OF} = 1/T_{1OFD} = B\nu^{-1} f_0^2(\nu/\nu_{cl})$	[19, 21]
Isotropic phase	$1/T_{1OF} = 1/T_{1OFS} = C/(\nu_{cl})^{1/2} \times \sum_{p=1}^{2} p^2/(1 + [1 + (p\nu/\nu_{cl})^2]^{1/2})^{1/2}$	[5, 17, 19]
Self-diffusion (SD)		
All phases	$1/T_{1SD} = D\tau_S f_S(\nu, \tau_S)$	[6, 10, 25]
Molecular rotation (R)		
All phases	$1/T_{1R} = E\tau_R f_R(\nu, \tau_R)$	[6, 10, 25]

System		Order fluctuation: Nematic $A/s^{-3/2}$	Nematic ν_{cl}/Hz	Smectic B/s^{-2}	Smectic ν_{cl}/Hz	Isotropic $C/s^{-3/2}$	Isotropic ν_{cl}/Hz	Self-diffusion D/s^{-2}	Self-diffusion τ_S/s	Rotation E/s^{-2}	Rotation τ_R/s
PAA	125°C	700	500	–	–	–	–	4.0×10^{9}	1.7×10^{-10}	–	–
PAA	135°C	–	–	–	–	950	$1.4\ 10^{7}$	3.8×10^{9}	1.4×10^{-10}	5.0×10^{6}	3.5×10^{-11}
MBBA	18°C	3500	800	–	–	–	–	1.1×10^{10}	2.4×10^{-10}	2.5×10^{9}	3.5×10^{-9}
CB7	32°C	4600	5500	–	–	–	–	2.4×10^{10}	1.3×10^{-10}	7.5×10^{8}	2.5×10^{-9}
PCH7	47°C	4900	7300	–	–	–	–	3.6×10^{10}	1.0×10^{-10}	1.1×10^{8}	5.0×10^{-9}
CCH7	48°C	21000	4000	–	–	–	–	3.2×10^{10}	5.0×10^{-10}	1.2×10^{8}	1.0×10^{-8}
CCH7	73°C	10500	3500	–	–	–	–	2.1×10^{10}	3.0×10^{-10}	7.5×10^{8}	3.0×10^{-9}
TBBA	185°C	–	–	14000	400	–	–	1.4×10^{9}	3.5×10^{-10}	1.5×10^{8}	1.0×10^{-9}
TBBA	205°C	1500	200	–	–	–	–	1.9×10^{10}	2.0×10^{-11}	2.0×10^{8}	0.5×10^{-9}

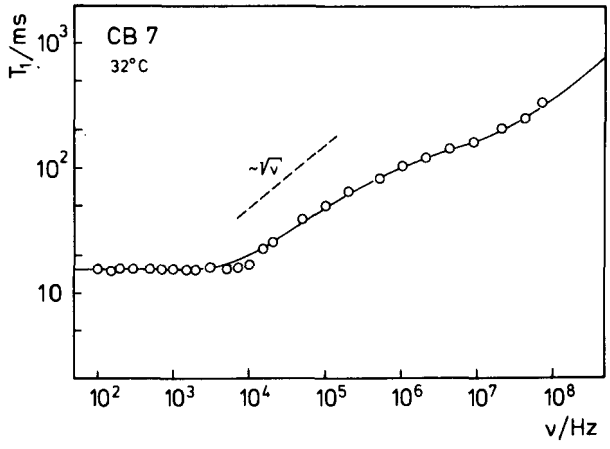

Figure 8. Proton relaxation dispersion $T_1(\nu)$ for nematic CB7 [19, 20]. The solid line is a model fit which, in addition to the OFD contribution including frequency cut-offs, takes into account relaxation by self-diffusion and molecular rotation. Details are summarized in table 2.

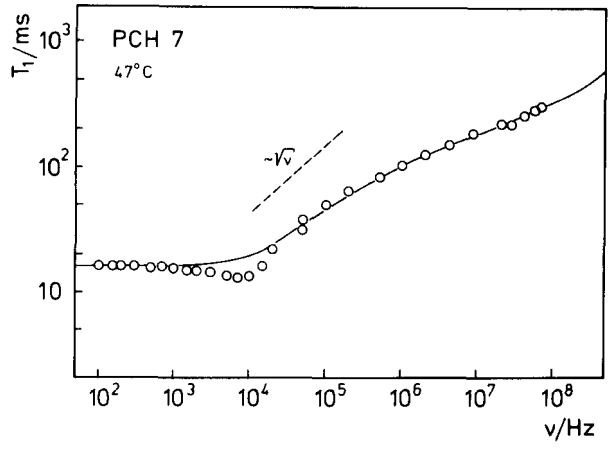

Figure 9. Proton relaxation dispersion $T_1(\nu)$ for nematic PCH7 [19, 20]. Details of the model fitting as in figure 8 are given in table 2.

(ii) The proton relaxation rate due to OFD differs by more than two orders of magnitude for the systems studied by us.

(iii) Preliminary measurements of deuteron $T_1(\nu)$ in MBBA-d_{13} also indicate a strong low-field dispersion.

More details will be described elsewhere. The first point is illustrated in figure 11 for MBBA (4-methyoxybenzylidene-4′-*n*-butylaniline) [19]. The $\nu^{1/2}$-contribution (OFD) at low frequencies is clearly recognized together with the two competing contributions at high frequencies, in this case self-diffusion and a molecular rotation not fully understood. An interesting finding is the circumstance that molecular rotation is stronger than self-diffusion, so that it will also be effective for deuteron relaxation, where, of course, intermolecular interactions are almost negligible. The second point is illustrated in figure 12, which shows the greatly different strengths of

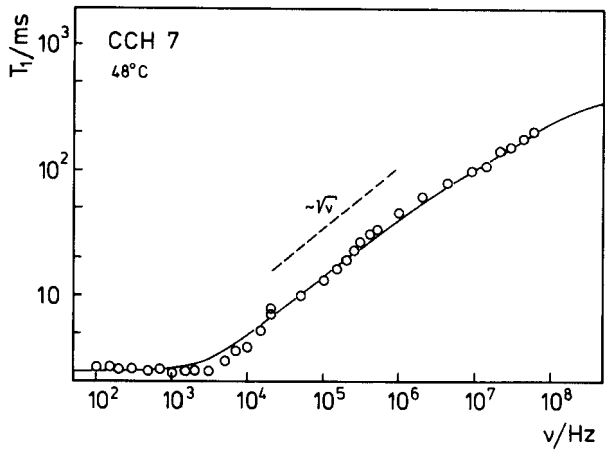

Figure 10. Proton relaxation dispersion $T_1(\nu)$ for nematic CCH7 [19, 20]. Details of the model fitting as in figure 8 are given in table 2.

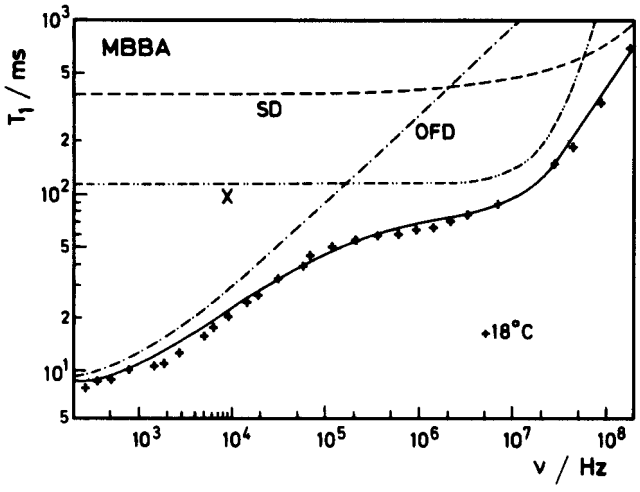

Figure 11. Proton relaxation dispersion $T_1(\nu)$ for nematic MBBA [10, 19] and model fit showing the three individual contributions to the dispersion profile: order fluctuation of the director (OFD), self-diffusion (SD) and molecular rotation about the short axis (X). Details of the fitting are given in table 2.

the $\nu^{1/2}$-contribution for some common nematic molecules (azoxybenzenes, cyanobiphenyls, phenyl-cyclohexanes and cyclo-cyclo-hexanes). Numerical values of the amplitude factor, A_{OFD}, determined at the same relative temperature are summarized in figure 13, they vary from 53 $s^{-3/2}$ in PAA-d_8 to 10 500 $s^{-3/2}$ in CCH7. What does this mean? We cannot establish a relation to either the central structure or the kind of end groups, yet the answer is simple. If we consider the various microscopic and macroscopic parameters reflected by A_{OFD}, namely on the one hand the spin pair separations and orientations and on the other hand the viscoelastic constants, we find an astonishingly good agreement with the theoretical predictions [20] where the data are available and reliable. The maximum deviation is less than a factor of two, but unfortunately it is largest for PAA, though here the underlying parameters are known most precisely. So there still remain open questions.

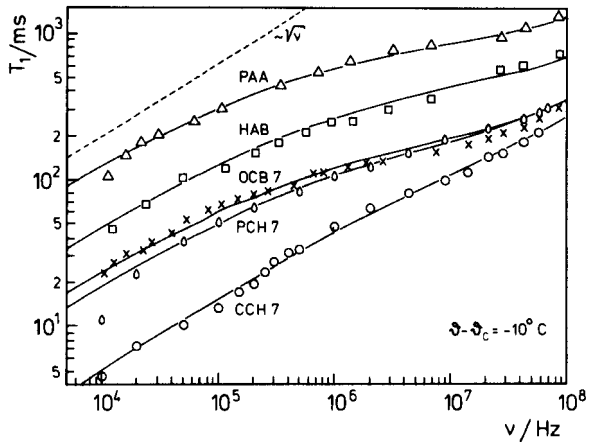

Figure 12. Proton relaxation dispersion $T_1(\nu)$ for some nematogens showing the different strength of the OFD contribution at low Larmor frequencies [20]. The measurements are compared at temperatures of 10°C below the individual clearing points T_c. The solid lines are model fits which, in addition to the OFD contribution, take into account relaxation by self-diffusion and molecular rotation [10, 20].

$\frac{1}{T_1} = A\nu^{-1/2} + \frac{1}{T_1'}$ $\quad \vartheta - \vartheta_{NI} = -10°C$

Substance		$A / s^{-3/2}$
PAA-d_8		53
PAA		613
PAA-d_6	R-⟨⟩-N=N(O)-⟨⟩-R'	970
PAB		1670
HAB		1570
MBBA		3160
MBBA-d_6	R-⟨⟩-C(H)=N-⟨⟩-R'	5930
MBBA-d_{13}		7940
OCB 5		3080
OCB 6	R-O-⟨⟩-⟨⟩-CN	2680
OCB 7		2760
OCB 8		2593
CB 7	R-⟨⟩-⟨⟩-CN	4600
PCH 7	R-⟨⟩-⟨⟩-CN	4900
CCH 7	R-⟨⟩-⟨⟩-CN	10500

Figure 13. Comparison of the order fluctuation relaxation factor $A = A_{OFD}$ as defined by equation (1) for numerous nematogens studied in this work [17–20].

Only very few relaxation dispersion measurements have been performed so far for smectic mesophases, nevertheless even these few studies provide an essentially new argument about the importance of collective motions. It was first pointed out by Vilfan *et al.* [21] and later by Marqusee *et al.* [22] that if in layered systems the propagation of the order fluctuation is restricted to the plane of the layer, i.e. to two dimensions, the square-root law should change to a linear frequency dependence

$$\frac{1}{T_{1\,\mathrm{OFD}}} = \frac{B_{\mathrm{OFD}}}{\nu^{1}}, \tag{2a}$$

with

$$B_{\mathrm{OFD}} = \tfrac{9}{32}\gamma^4\hbar^2 k \frac{TS^2}{d^6 K\zeta} \frac{(3\cos^2\alpha - 1)}{4} f(\beta), \tag{2b}$$

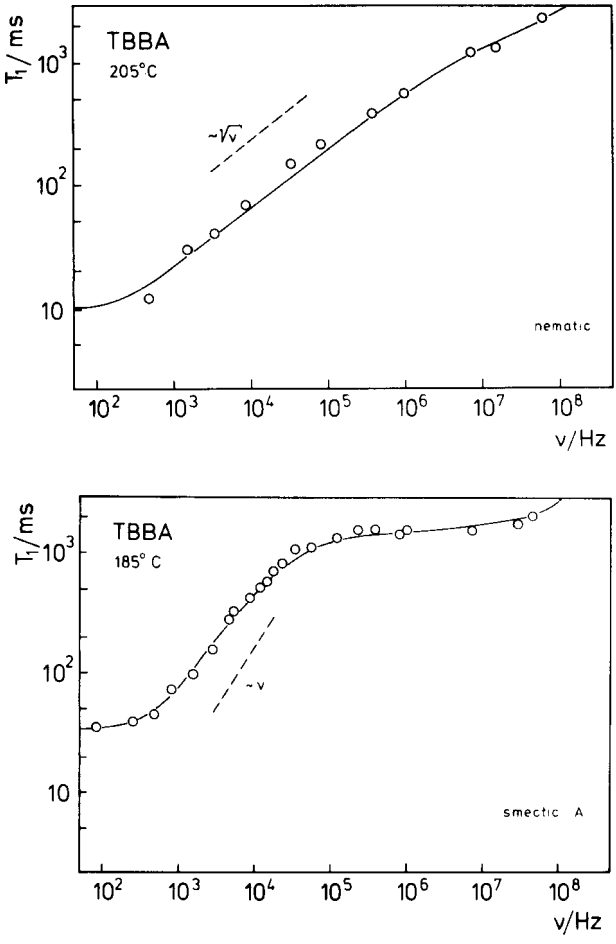

Figure 14. Larmor frequency dependence of the proton relaxation time T_1 in nematic and smectic-*A* TBBA [23]. Top: nematic phase with square-root dispersion profile according to equation (1 *a*). Bottom: smectic *A* phase with linear dispersion profile according to equation (2 *a*). The solid lines are model fits which, in addition to the OFD contribution including frequency cut-offs, take into account relaxation by self-diffusion and molecular rotation. Details are summarized in table 2.

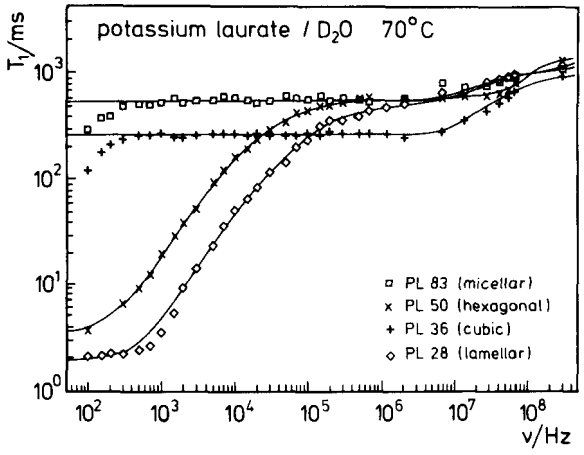

Figure 15. Proton relaxation dispersion $T_1(\nu)$ for the micellar, hexagonal, cubic and lamellar phase of lyotropic potassium laurate-D_2O mixtures [26]. The linear profile, according to equation (2a), is absent for the isotropic systems. Details of the model fits (solid lines), which again combine relaxation by order fluctuations, self-diffusion and molecular rotation, have been described previously [26].

where ζ means a coherence length perpendicular to the layers and the other notation is the same as in equation (1). Exactly this behaviour is observed by field-cycling studies where the measurements have been extended to sufficiently low Larmor frequencies. For instance, the T_1 dispersion in the smectic A phase of terephtalbis(4-*n*-butylaniline) (TBBA) clearly exhibits the $T_1 \sim \nu^1$ regime instead of the typical $\nu^{1/2}$ regime seen in the nematic phase of this mesogen [23] (see figure 14). Again two additional relaxation mechanisms (self-diffusion and molecular rotations) are necessary to interpret the experimental data quantitatively. Such a change in the dispersion profile has also been described for a 4-*n*-alkanoyl-benzylidene-4′-aminobenzene (C_{12}-AA) [24] as well as for 4-*n*-alkoxy-4′-cyanobiphenyl (OCB) mixtures [25]. As is expected, the linear frequency dependence is even better developed in lyotropic systems such as lamellar potassium laurate–water mixtures (see figure 15), namely because in this case the smectic-type layers are almost decoupled by the water interface. Note the circumstance that the $T_1 \sim \nu^1$ divergence completely disappears for the cubic and micellar structure and thus strongly supports the concept of smectic order fluctuations in the lamellar system. Somewhat surprisingly, the $T_1 \sim \nu^1$ law is also verified for the hexagonal phase of this system (see figure 15), which implies that the mode propagation must be restricted to two dimensions. Using this concept we can easily understand the reduced relaxation rate compared with the data for the lamellar phase by the different order parameters [26].

The last example (see figure 16) presents measurements of the proton relaxation dispersion in the liquid-crystalline phase of the phospholipid-water model membrane system dimyristoylglycerophosphocholine (DMPC–D_2O), a system violently disputed in the literature [27, 28]. DMPC–water mixtures undergo three well-known phase transitions as a function of temperature and water content between a so-called liquid-crystalline (L_α), an intermediate (P_β) and a gel ($L_{\beta'}$) phase. All these structures are lamellar with different molecular orientations and different degrees of order. Using a non-polar solvent as, for example, $CDCl_3$ we can also produce an isotropic solution.

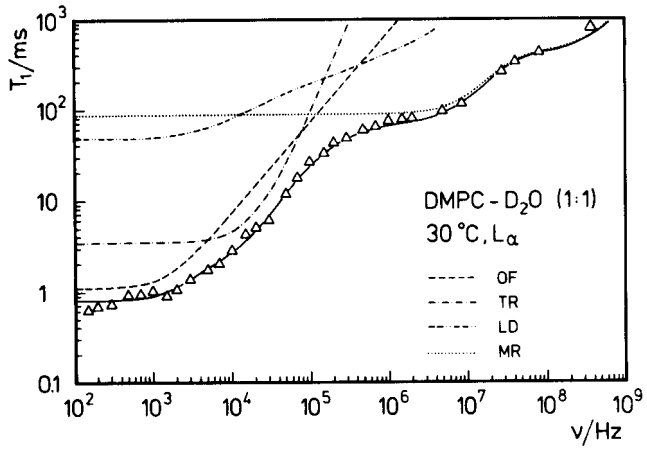

Figure 16. Proton relaxation dispersion $T_1(\nu)$ for the lamellar liquid crystalline phase (L_α) of the model membrane system dimyristoylglycerophosphocholine-water (DMPC–D_2O) [28]. The linear profile according to equation (2*a*) is observed in the frequency range $10^3\,\text{Hz} \lesssim \nu \lesssim 10^5\,\text{Hz}$. A detailed analysis of the data reveals at least three additional relaxation mechanisms, namely segmental molecular reorientations (MR), lateral self-diffusion in the layers (LD), and overall molecular rotations induced by translational jumps on a curved surface (TR). The diagram shows both the individual contributions (dashed lines) and the resulting model fit (solid line) [28].

Our extensive $T_1(\nu)$ results demonstrate that, in contrast to frequent suggestions in the literature [27], collective molecular reorientations contribute to the relaxation process only at rather low Larmor frequencies in the kHz regime, whereas the conventional high frequency MHz range is dominated by the reorientation of individual molecules. The order fluctuations are detected by the characteristic $T_1 \sim \nu^1$ dispersion profile in the liquid-crystalline phase and to a much smaller degree also in the intermediate phase; this linear profile is completely absent for both the isotropic and the gel mixtures. Both findings provide important support for the validity of the Blinc–Marqusee model [21, 22]. More than that, by making use of the molecular parameters involved in equation (2), we can show that the order fluctuation contribution has a reasonable magnitude [28], and by combining the collective modes with faster non-collective reorientations (lateral self-diffusion and various molecular rotations) we can give a quantitative interpretation of the whole relaxation dispersion profile [28].

4. Zero-field spectra of liquid crystals

As emphasized in § 2, fast field-cycling makes it possible not only to measure the longitudinal relaxation time T_1, but any N.M.R. parameter which is field dependent by combining field switching with adequate rf irradiation. In recent years it was pointed out by Pines *et al.* [15] that the measurement of spectra in a low- or zero-field, in practice by the Fourier transform of the transverse magnetization decay, should give informations not or not easily obtained from conventional high-field experiments. This is mainly due to the fact that the dipolar or quadrupolar splittings in zero-field spectra no longer depend on the orientation of spin pairs or electric field

gradients relative to an external Zeeman field $\mathbf{B}_0$, so that a distribution of angles does not broaden the lines. So we expect to have a means to better disentangle effects originating from the orientation and the motion of the considered molecules, a fundamental aspect of spectra of liquid crystals.

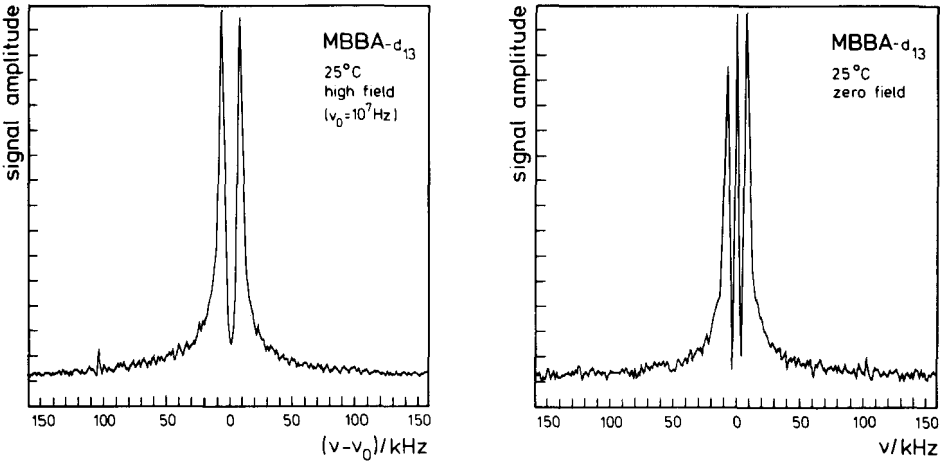

Figure 17. Proton spectra of nematic MBBA-d_{13} at 25°C [29]. Left: high-field doublet at a Larmor frequency $\nu_0 = 10^7$ Hz. Right: zero-field triplet at $\nu_0 < 50$ Hz. The line splitting $\Delta\nu$ is identical in both cases.

Our experiments performed so far with that aim are somewhat disappointing, particularly in view of the great technical efforts needed to measure such spectra in the presence of the rather short T_1 times. Let us explain a typical result for a simple example, namely chain deuteriated MBBA-d_{13}, where only ring proton pairs contribute to the signal. As expected, the dipolar interaction of neighbouring protons produce a doublet in the high-field and a triplet in the zero-field [15, 29] experiment (see figure 17). As also expected, the splitting $\Delta\nu$ between the outer lines is the same in both cases, which means that according to [1, 2, 15]

$$\Delta\nu = \frac{3}{2}\frac{\gamma^2\hbar}{d^3} S \frac{(3\cos^2\alpha - 1)}{2}, \tag{3}$$

the order parameter S is identical on the time scales of both Lamor frequencies. But we do not find a line narrowing in the zero-field spectrum as a consequence of the vanishing effect of the orientational distribution of spin pairs, which may be partly due to the circumstance that T_1 is much shorter under low-field than under high-field conditions, and possibly also partly results from technical difficulties of the new method [29].

However, examining finer details of the spectra finally reveals results only visible under zero-field conditions (see figure 18). If we compare the high- and low-field spectrum as a function of temperature, again for MBBA-d_{13}, we first recognize that the splittings and hence the order parameter decreases with higher temperature in the same way, within the experimental accuracy. This does not provide any new information! But in addition, the zero-field lines show a strong variation of the intensity ratio of the outer to the central lines. It is almost inverted despite the small mesophase range. What does this mean? Using the Hennel formalism for zero-field N.M.R. of

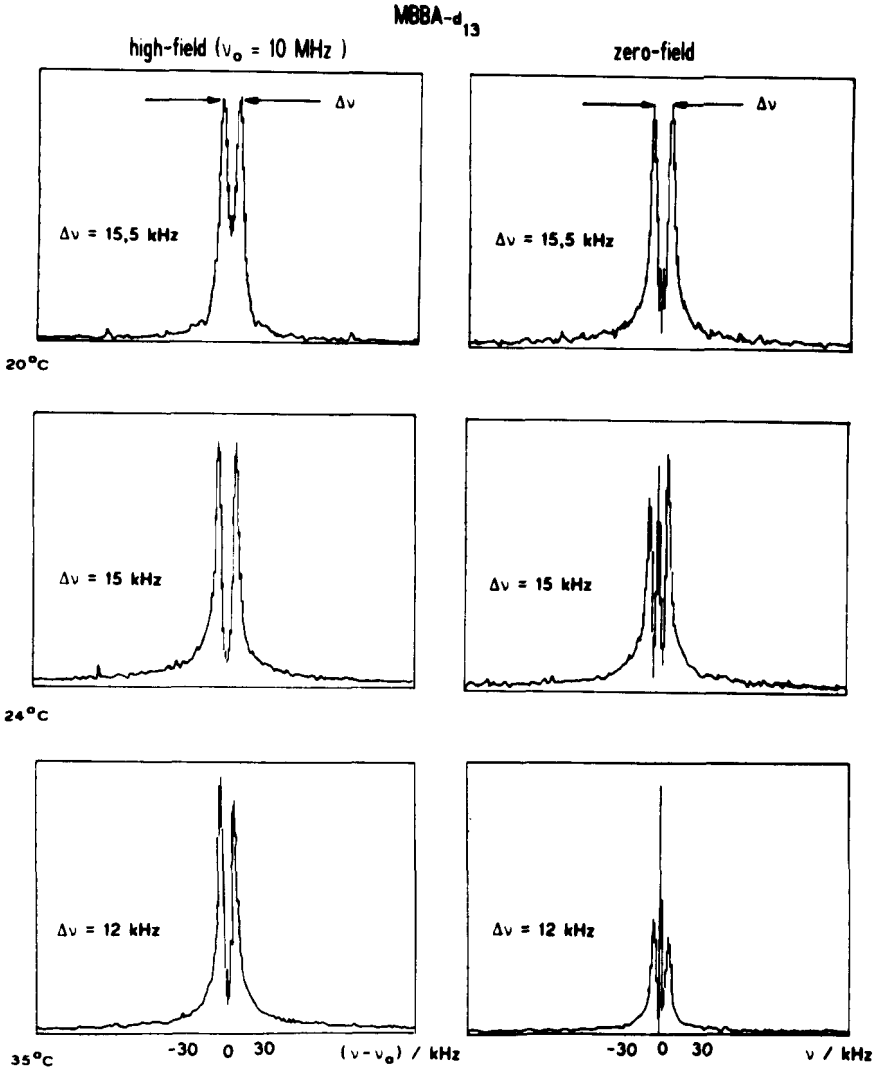

Figure 18. Temperature dependence of the high-field and zero-field proton spectra of nematic MBBA-d_{13} [29]. Note the strong intensity variations of the outer and central lines under zero-field condition.

rotating spin pairs [30], the change can be interpreted quantitatively by a slow reorientation of the proton pairs around the short molecular axis with a jump rate near 10^4 Hz, which slightly increases at higher temperatures. So the slow motions seen in the T_1 dispersion are to some extent also visible in the spectrum. Similar intensity changes have also been observed, though less dramatic, in non-deuteriated MBBA, where the spectrum is more complex due to the different spin pairs, and in deuteriated and non-deuteriated PAA samples [29]. Details will be described elsewhere.

The authors thank Dipl. Phys. E. Rommel, Dipl. Phys. K. H. Schweikert and Dipl. Phys. G. Osswald for helpful comments to this work. The financial support by the Deutsche Forschungsgesellschaft is gratefully acknowledged.

References

[1] LIPPMANN, H., and WEBER, K. H., 1957, *Ann. Phys.*, **20**, 265.
[2] SAUPE, A., and ENGLERT, G., 1964, *Z. Naturf.* (*a*), **19** 172.
[3] PINCUS, P., 1969, *Solid St. Commun.*, **7**, 415.
[4] BLINC, R., HOGENBOOM, D. L., O'REILLY, D. E., and PETERSON, E. M., 1969, *Phys. Rev. Lett.*, **23**, 969.
[5] For example: (a) DOANE, J. W., and JOHNSON, D. L., 1970, *Chem. Phys. Lett.*, **6**, 291. (b) UKLEJA, P., PIRS, J., and DOANE, J. W., 1976, *Phys. Rev.* A, **14**, 414. (c) FREED, J. H., 1977, *J. chem. Phys.*, **66**, 4183.
[6] ABRAGAM, A., 1962, *The Principles of Nuclear Magnetism* (Oxford University Press).
[7] ZUPANČIČ, I., ŽAGAR, V., ROŽMARIN, M., LEVSTIC, I., KOGOVŠEK, F., and BLINC, R., 1976, *Solid St. Commun.*, **18** 1591.
[8] VILFAN, M., and ŽUMER, S. (private communication).
[9] KIMMICH, R., 1980, *Bull. Magn. Reson.*, **1**, 195.
[10] NOACK, F., 1986, *Prog. Nucl. Magn. Reson. Spectrosc.*, **18**, 171.
[11] POUND, R. V., 1951, *Phys. Rev.*, **81**, 156.
[12] REDFIELD, A. G., FITE, W., and BLEICH, H. E., 1968, *Rev. scient. Instrum.*, **39**, 710.
[13] ROMMEL, E., MISCHKER, K., OSSWALD, G., SCHWEIKERT, K. H., and NOACK, F., 1986, *J. magn. Reson.*, **70**, 219.
[14] SCHWEIKERT, K. H., KRIEG, R., and NOACK, F., *J. magn. Reson.* (in the press).
[15] BIELECKI, A., ZAX, D. B., ZILM, K. W. and PINES, A., 1986, *Rev. scient. Instrum.*, **57**, 393.
[16] For example: (a) DOANE, J. W., and VISINTAINER, J. J., 1969, *Phys. Rev. Lett.*, **23**, 1421. (b) WEGER, M., and CABANE, B., 1969, *J. Phys.*, **30**, C4-72. (c) VILFAN, M., BLINC, R., and DOANE, J. W., 1972, *Solid St. Commun.*, **11**, 1073.
[17] WÖLFEL, W., NOACK, F., and STOHRER, M., 1975, *Z. Naturf.* (*a*), **30**, 437.
[18] WÖLFEL, W., 1977, Thesis, Universität Stuttgart.
[19] GRAF, V., 1980, Thesis, Universität Stuttgart.
[20] NOTTER, M., 1986, Diplomarbeit, Universität Stuttgart.
[21] BLINC, R., LUZAR, M., VILFAN, M., and BURGAR, M., 1975, *J. chem. Phys.*, **63**, 3445.
[22] MARQUSEE, J. A., WARNER, M., and DILL, K. A., 1984, *J. chem. Phys.*, **81**, 6404.
[23] MUGELE, TH., GRAF, V., WÖLFEL, W., and NOACK, F., 1980, *Z. Naturf.* (*a*), **35**, 924.
[24] KRÜGER, G. J., SPIESECKE, H., VAN STEENWINKEL, R., and NOACK, F., 1977, *Molec. Crystals liq. Crystals*, **40**, 103.
[25] SCHWEIKERT, K. H., 1985, Diplomarbeit, Universität Stuttgart.
[26] KÜHNER, W., ROMMEL, E., and NOACK, F., 1987, *Z. Naturf.* (*a*), **42**, 127.
[27] BROWN, M. F., and WILLIAMS, G. D., 1985, *J. biochem. biophys. Meth.*, **11**, 71.
[28] ROMMEL, E., NOACK, F., MEIER, P., and KOTHE, G., *J. phys. Chem.* (in the press).
[29] (a) WEIß, W., 1987, Diplomarbeit, Universität Stuttgart. (b) WEIß, W., KRIEG, R., and NOACK, F., 1987, 9th GDCh Diskussionstagung, Hünfeld.
[30] HENNEL, J. W., BIRCZYŃSKI, A., SAGNOWSKI, S. F., and STACHUROWA, M., 1985, *Z. Phys.* B, **60**, 49.